Quantitative Measurement of Cation-Mediated Adhesion of DNA to Anionic Surfaces

— Supporting Information

Xian Hao,[†,‡,§] Qufei Gu,[|,§] Christine Isborn,[†] Jesus Rodriguez Vasquez,[†] Makenzie Provorse Long*,[¶] and Tao Ye*,[|,†]

[†] Department of Chemistry and Biochemistry, School of Natural Sciences, University of California, Merced, California, 95343 United States.

[‡] School of Public Health &Jiangxi Provincial Key Laboratory of Disease Prevention and Public Health, Nanchang University, Nanchang, Jiangxi, 330006, China.

[|]Materials and Biomaterials Science and Engineering, School of Engineering, University of California, Merced, California, 95343, United States.

¶Department of Chemistry and Biochemistry, Creighton University, Omaha, Nebraska, 68178, United States.

* E-mail: tao.ye@ucmerced.edu (T.Y.), makenzielong@creighton.edu (M.P.L.)

[§] These authors contributed equally to the work.

Table of Contents

Experimental Materials and Methods

Synthetic oligonucleotides used:

Name	DNA Sequences & Modifications
DNA anchor strand for CuAAC click chemistry	5'-(Ak)-gctacctcgtgagcagtcagtacgttttt/(C11-SS)-3'
DNA anchor strand for hydrazone crosslinking	5'-gtgagtgatggcaagtatggatgattttt/(C11-SS)-3'
Forward primer for CuAAC click chemistry	5'-(Az)/cgtactgactgctcacgaggtagc/(C3)/tctgaactgtttaaagcatttgaggg-3'
Reverse primer for CuAAC click chemistry	5'-acagcttgataccgatagttgcg-3'
Forward primer for hydrazone crosslinking	5'-tcatccatact/(dU)/accatcactcac/(C3)/tctgaactgtttaaagcatttgaggg-3'
Reverse primer for hydrazone crosslinking	5'-acagcttgataccgatagttgcg-3'

Abbreviations used above: (Ak) = alkyne; (Az) = azide; (dU) = deoxyuracil; (C3) = propyl spacer; (C11-SS) = undecyl disulfide. The disulfide-modified DFNA anchor strand was purchased from Biosearch technologies (Novato, California, USA) and all other synthetic oligonucleotides were purchased from Integrated DNA Technologies (Coralville, Iowa, USA). The purity of the commercial oligonucleotides was verified by the manufacturers using mass spectrometry, and the DNA was used without further purification unless otherwise stated.

Tethering anchor DNA to the AFM tip:

Au-coated Si_3N_4 AFM tips (Model NPG-10, Bruker, Santa Barbara, CA, USA) with a nominal spring constant of ~0.06-0.12 N/m were cleaned by first exposing the tips to the ultraviolet (UV) radiation for 20 min to remove organic contaminants and then immersing them in hot ethanol (~75°C) for 20 min to reduce oxidized Au that may have formed during UV exposure. The cleaned Au tips were incubated with a 1 mM ethanolic solution of MUDA (Millipore-Sigma, St. Louis, MO, USA) for 30 min to form a SAM, followed by rinsing 3 times with the 1 × TAE solution. To insert the DNA anchor strands, Au tips with preassembled SAM were immersed overnight in a solution of 50 nM purified, thiolated DNA anchor strand purified using a QIAquick Nucleotide Removal Kit (QIAGEN, Germantown, MD, USA), 1 × TAE, 2 mM TCEP, 2 mM $MgAc_2$ and 50 mM NaAc in a Teflon beaker.[1] The Teflon beaker was sealed with parafilm and backfilled with nitrogen.

Generation of target DNA:

To linearize the phage vector, a 10 ng/μL circular M13mp18 RF I (New England Biolabs, Ipswich, MA, USA) was mixed with 200 μg/μL BSA, 20 units of EcoRI enzyme, and 1× EcoRI buffer and incubated at 37 °C for 2 h. To denature the enzymes, the mixture was heated up to 65 °C for 20 min and cooled down at 4 °C in a thermal cycler. For PCR amplification, a solution of 50 pg/μL of linearized M13mp18 RF I dsDNA template, 200 nM of forward/reverse primers (Figure S1) and OneTaq 1 × master mixed with the standard buffer was first heat up to 95 °C for 3 min, followed by 34 cycles of 3 s at 95 °C, 45 s at 53 °C, and 2 min 30 s at 72 °C, finishing with 10 min at 72 °C. The PCR products were held at 4 °C and purified with the QIAquick PCR Purification Kit (QIAGEN, Germantown, MD, USA).

Hybridization of anchor and target DNA:

The Au tips were rinsed 3 times with the 1 × TAE solution prior to hybridization step. The Au tips were then immersed in a solution containing 80 nM dsDNA with a 24-base single stranded sticky end, 1 × TAE, 1 mM SDS, 2 mM $MgAc_2$ and 1 M NaAc in a Teflon beaker for 1 h. The dsDNA used here was 1031 bp in length and PCR-amplified from the linearized M13mp18 RF I dsDNA template. After hybridization, the tips were then rinsed three times with the 1 × STAE buffer.

DNA functionalization of AFM cantilever:

Figure S2 illustrates how a dsDNA molecule is covalently tethered to an AFM tip using DNA templated crosslinking. Thiolated anchor strand DNA molecules with a reactive group were inserted into surface defects of a host SAM of MUDA on a gold-coated AFM tip (B1), allowing the anchor DNA to capture the long target DNA with a complementary sequence (B2), and then covalently crosslinking the strands (B3). Two different conjugation methods were used: Cu(I)-catalyzed azide-alkyne cycloaddition (CuAAC) click chemistry[2] and hydrazone crosslinking chemistry.

CuAAC click chemistry: The anchor strand bearing an alkyne group was purchased from Biosearch technologies. The target stand with a terminal azide group was generated via PCR with a forward primer bearing an azide group. After hybridization, the DNA was cross-linked by immersing the AFM tips in a solution containing 200 μM $CuSO_4$, 200 μM Tris(3-hydroxypropyltriazolylmethyl) Amine (THPTA, Sigma Aldrich, St. Lois, MO, USA), 2 mM sodium ascorbate (Sigma Aldrich, St. Lois, MO, USA), PBS (pH 7), 10% DMSO for 15 min in a Teflon beaker. The Teflon beaker was sealed with parafilm and backfilled with nitrogen. The AFM tips were then stored in STAE buffer.

Hydrazone crosslinking: To generate an abasic site on target strand, enzymatic cleavage of the deoxyuracil (dU) base was performed according to a previously published protocol.[3] A solution of dU-containing DNA target, 2.5 units of Uracil DNA Glycosylase enzyme (UDG, New England Biolabs, Ipswich, MA, USA), and 1 × UDG reaction buffer (20 mM Tris-HCl, 1 mM EDTA, 1 mM DTT, pH 8) was held at 37°C for 1 hr. The target DNA solution was then purified using a QIAquick PCR Purification Kit and used immediately after purification. The addition of an N^4-amino group to the deoxycytosine (dC) base in the anchor DNA was performed following a previously published protocol.[3] A solution of 20 μM dC-containing DNA anchor, 4 M hydrazine monohydrochloride, 0.3 M sodium bisulfite, and 100 mM sodium phosphate buffer (pH 5) was held at 50°C for 3 hr and then stopped by addition of 3 vol of TET buffer (1 × TET = 100 mM Tris-HCl, 1 mM EDTA, 10 mM triethylamine, pH 10). The anchor DNA solution was then purified using Illustra NAP-5 columns (GE Healthcare Life Sciences, Pittsburgh, PA, USA) and used immediately after purification. After hybridization, the DNA was cross-linked by immersing the AFM tips in PBS

(pH 5) and heating to 50°C for 10 min. After heating, the AFM tips were cooled down to room temperature (~22°C) and stored in PBS (pH 5).

Speciation of Ni^{2+}

One potential complication is that acetate weakly binds to Ni^{2+}, obscuring the analysis. Assuming the stability constant of $[NiAc]^+$ to be 10,[4] about ~26% of Ni^{2+} cations were expected to complex with acetate with 100 mM Tris-Acetate added. Therefore, the decline of the adhesion force may originate from not only increasing electrostatic screening but also a lower availability of free Ni^{2+}. Despite the complication, these results nevertheless showed that Ni^{2+} mediates stronger DNA binding even with potentially lower availability of free Ni^{2+}. Another complication is that the addition of $Ni(Ac)_2$ slightly decreases the pH of the TAE buffer solution, which has a pH of 8.3. The pHs of the Ni^{2+} solutions are 8.15, 8.01, 7.83, 7.78, 7.68, 7.57 at 2.5 mM, 5 mM, 10 mM, 12.5 mM, 15 mM, and 20 mM, respectively. The reduced pH, in combination with the salt effect, ensures that nickel cations do not precipitate. Despite the pH reduction, the pH is well above the pKa of the MUDA SAM in divalent cations. Therefore, we assume near complete ionization of the carboxyl groups.

Additional discussion on DNA-surface interactions

While the lack of strong adhesion of DNA to neutral OH terminated SAM on gold shows that ICIs are not the main contributor to adhesion, our observation that adhesion is much stronger in a divalent cation buffer than a monovalent cation buffer is also inconsistent with ICIs being the main contributor to adhesion as the energy of ICIs scales quadratically with the amount of charges[5-6] and dsDNAs are half as charged in a divalent cation buffer as in a monovalent cation buffer according to the Manning's counterion condensation theory.[7] The lack of detectable contributions from ICIs can be rationalized by two key factors. First, the ICI energy is inversely proportional to the distance from the gold surface.[5-6] Hence, the MUDA SAM significantly reduces ICIs by separating DNA from the gold surface by more than 1 nm. Moreover, the ICIs are heavily screened by water molecules. Son *et al*.'s MD simulation study of ion adsorption onto a metal electrode showed that the ICIs are insignificant due to screening by water molecules.[8]

Another explanation of DNA-surface interaction is hydrogen bonding between the phosphate groups of the dsDNA and the protonated carboxyl groups on the surface. A control experiment done with 1 M NaAc and 2 M NaAc did not observe a plateau force (Figure S3). The lack of observable

adhesion forces in the monovalent cation buffer under high ionic strength conditions rules out hydrogen bonding as a major contributor to the adhesion force between DNA and the MUDA surface. Moreover, in a Ni^{2+} or Co^{2+} solution, the carboxyl groups are completely deprotonated and unable to hydrogen bond with phosphate groups.[9-11] Yet, strong adhesion energies, up to 6-7 k_BT/bp, were observed. That the adhesion forces are the strongest when few, if any, hydrogen bonds can form between DNA and deprotonated MUDA surface in Ni^{2+} and weakest when hydrogen bonds can readily form between DNA and protonated MUDA (in Na^{+}) shows that hydrogen bonding is not a main contributor to adhesion forces. Rather electrostatic interactions can readily account for the magnitude of DNA-surface interactions.[12]

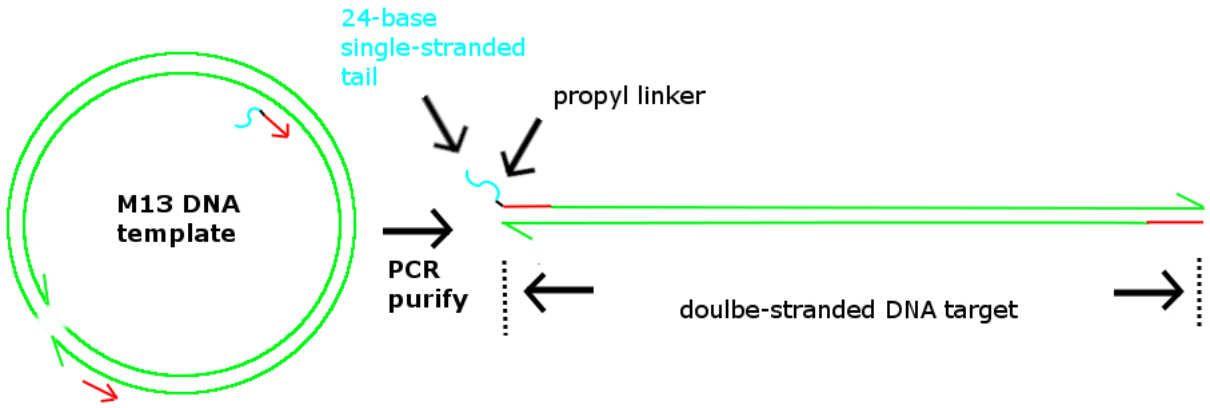

Figure S1. Schematic illustration of the generation of the double-stranded DNA targets via PCR with modified primers (primers in red).

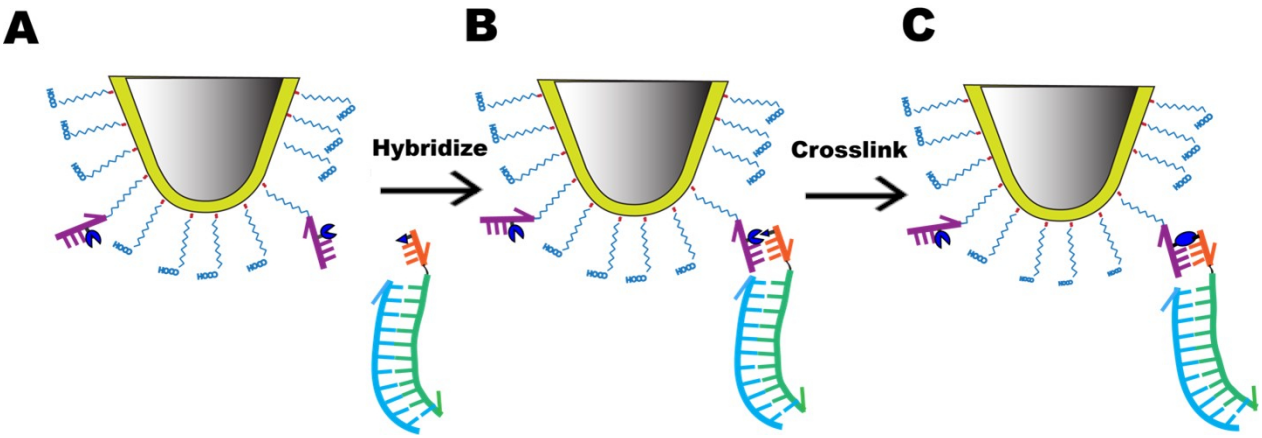

Figure S2. Schematic illustration of modification of AFM tip with long dsDNA. (A) The gold coated AFM tip is functionalized with 11-mercaptoundecanoic acid and thiolated DNA anchor strands that are modified with a reaction group. (B) Hybridization between an anchor strand and double stranded DNA with a single stranded tail bring two reactive groups together. (C) Reaction between the reactive groups crosslinks the two DNA strands, covalently linking the long DNA to the surface.

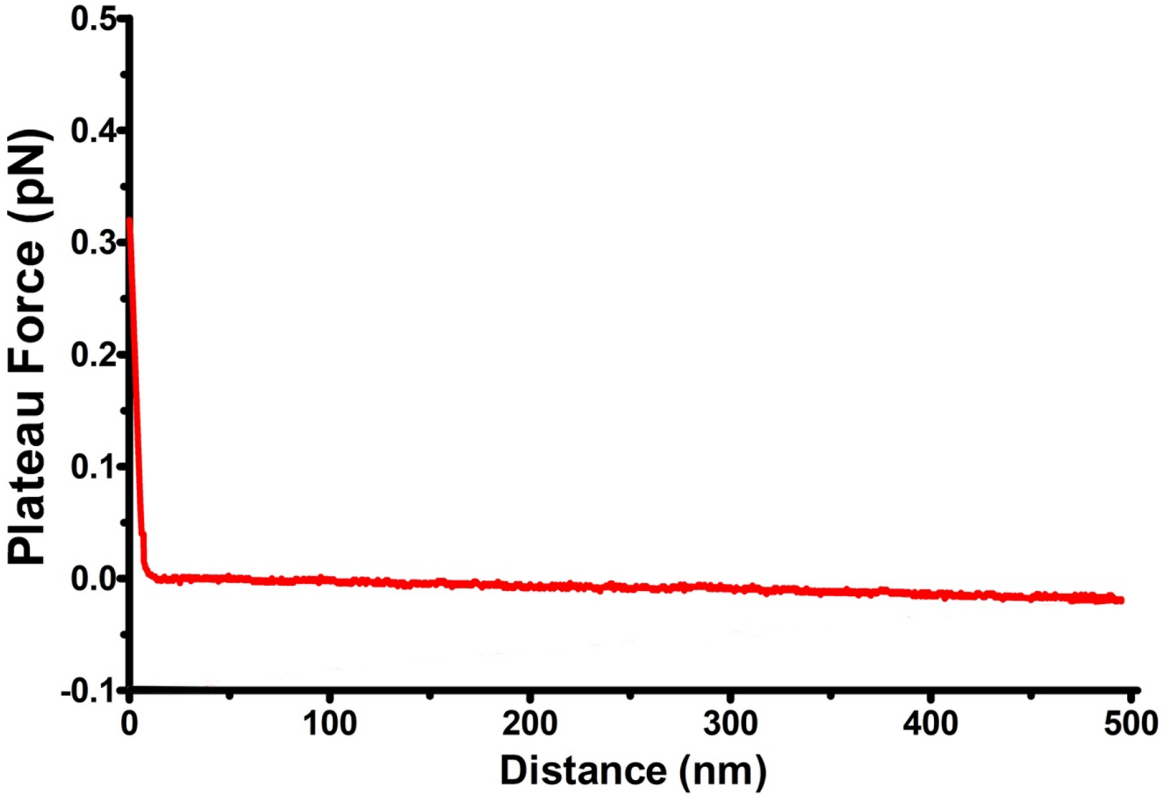

Figure S3. Representative force-distance curve of an AFM tip that is not functionalized with dsDNA.

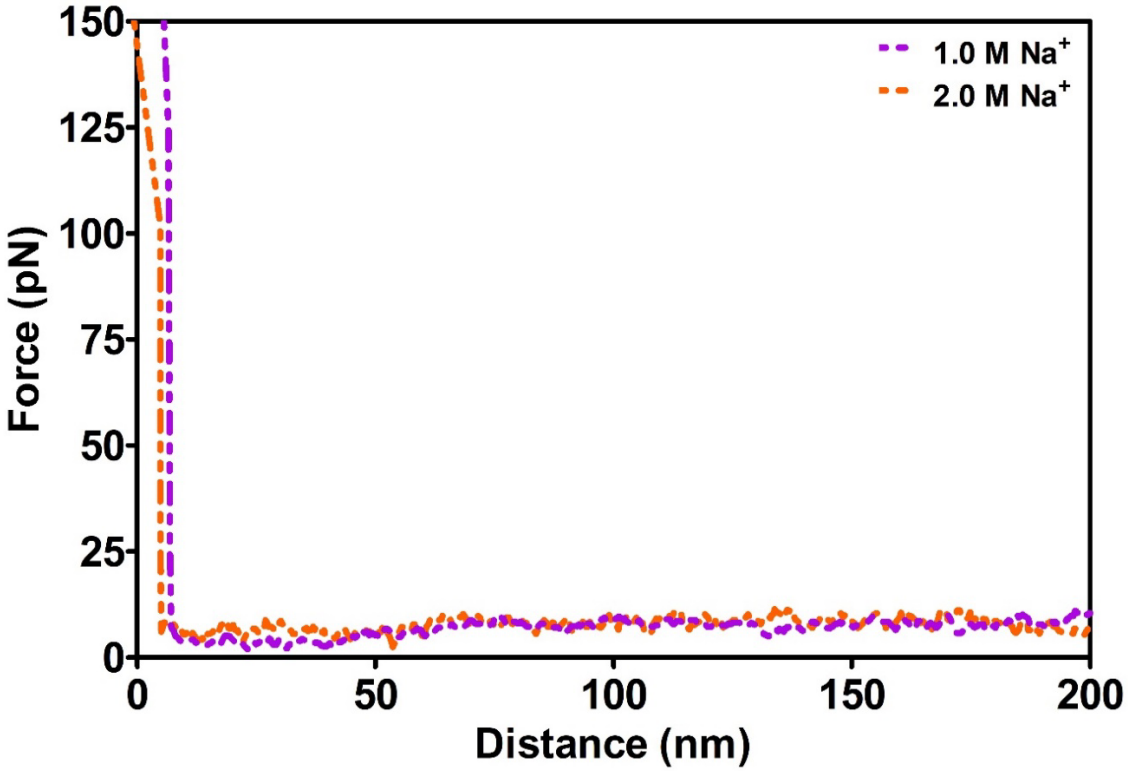

Figure S4. Representative force-distance curves of DNA tethered AFM tips in 1 M (purple) and 2 M (orange) NaAc buffer.

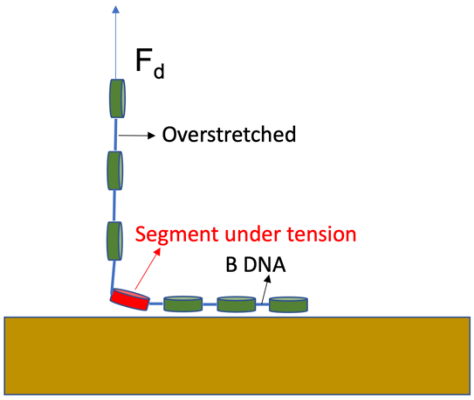

Figure S5. Model of DNA being peeled off the surface. The portion on the surface is not overstretched. And only one segment (like a single base-pair) is experiencing tension. After the segment leaves the surface, it can then be overstretched.

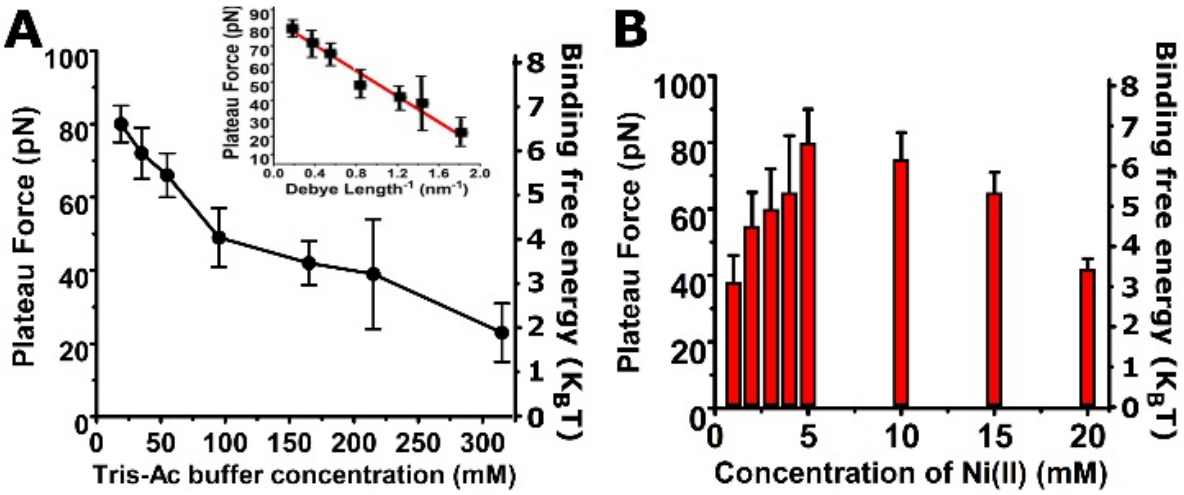

Figure S6. Effects of the buffer composition on the plateau force of dsDNA on MUDA SAM. (A) Plateau force/binding energy as a function of the ionic strength. The concentration of Ni^{2+} was held constant at 5 mM. The ionic strength was varied by adjusting the concentration of Tris-Ac. (B) Plateau force/binding energy as a function of the concentration of Ni(II) acetate. The concentration of Tris-Ac buffer was held constant at 4 mM.

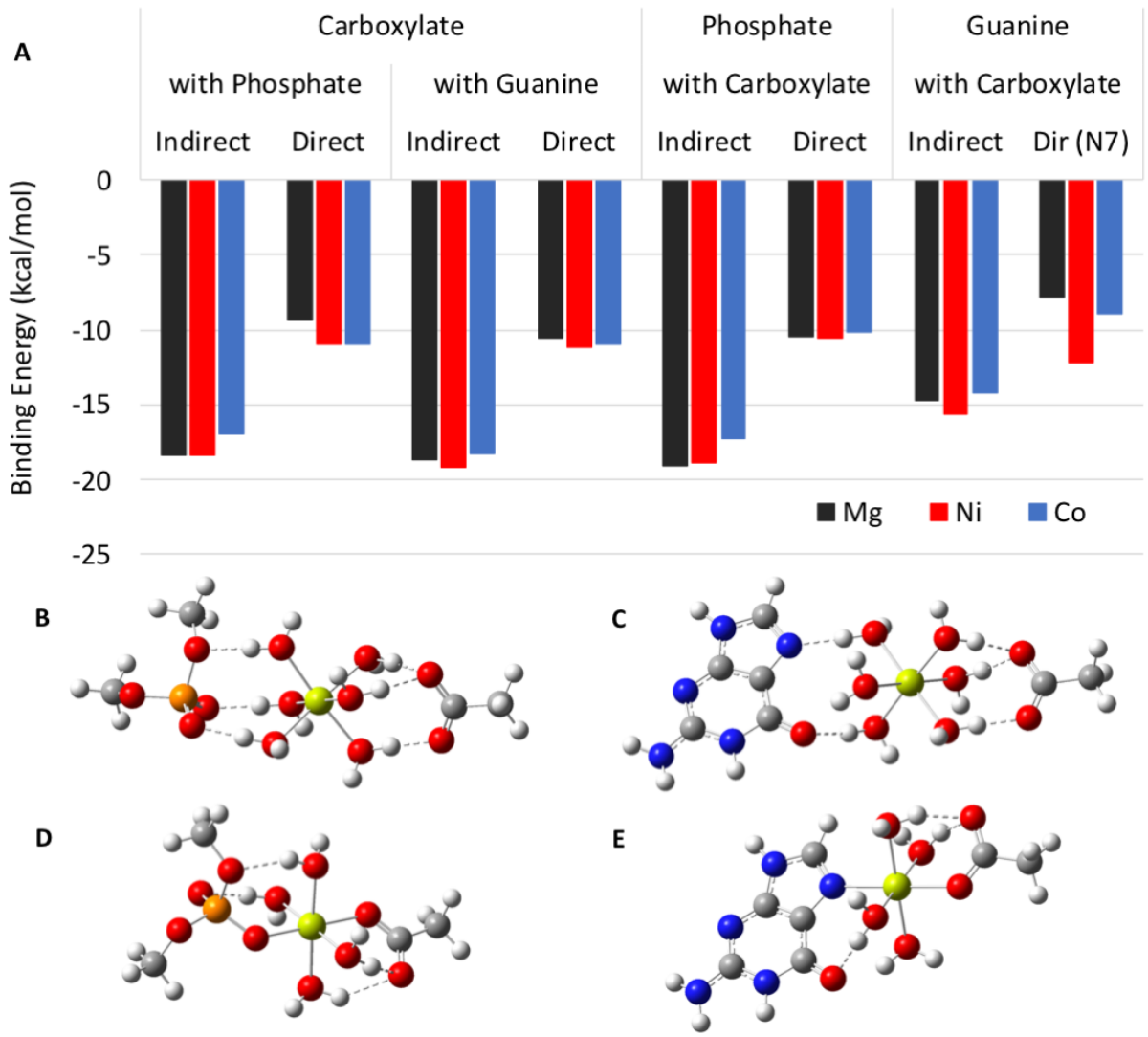

Figure S7. (A) Calculated binding energies (kcal/mol) of $[Mg(H_2O)_6]^{2+}$, $[Ni(H_2O)_6]^{2+}$, or $[Co(H_2O)_6]^{2+}$ indirectly and directly bound to carboxylate and phosphate or carboxylate and guanine at the B3LYP/6-311+g(d,p) level of theory with GD3BJ empirical dispersion. (B-E) Optimized geometries of the ternary Mg^{2+} complexes at the same level of theory. Mg, P, O, N, C, and H atoms are shown as yellow, orange, red, blue, grey, and white spheres, respectively.

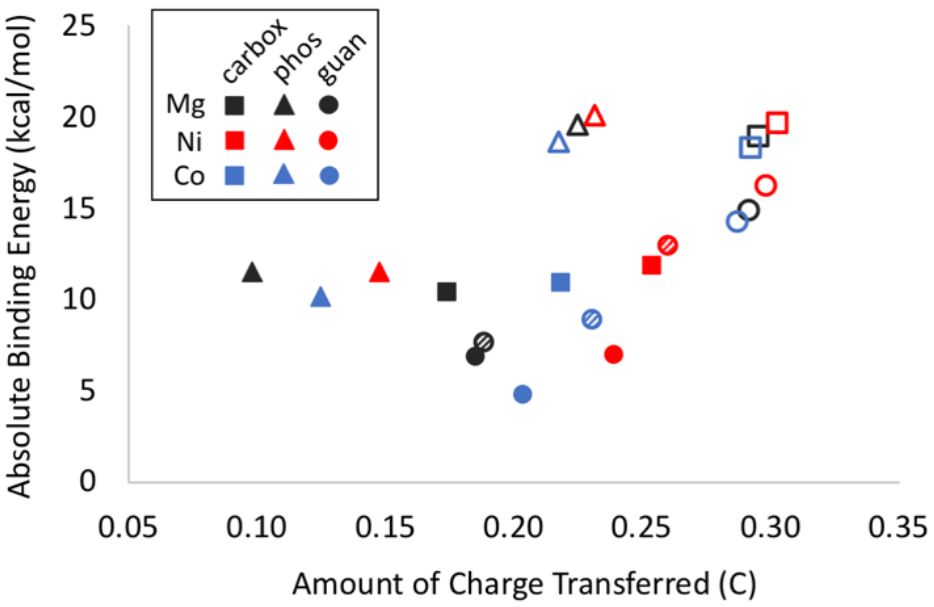

Figure S8. The absolute binding energy (kcal/mol) of $[Mg(H_2O)_6]^{2+}$, $[Ni(H_2O)_6]^{2+}$, or $[Co(H_2O)_6]^{2+}$ indirectly or directly bound to carboxylate (carbox), phosphate (phos), or guanine (guan) as a function of the amount of charge transferred in coulomb (C). Unfilled and filled shapes represent indirect and direct binding complexes, respectively. Direct binding at the N7 and O6 atoms of guanine are shown as pattern-filled and solid-filled circles, respectively.

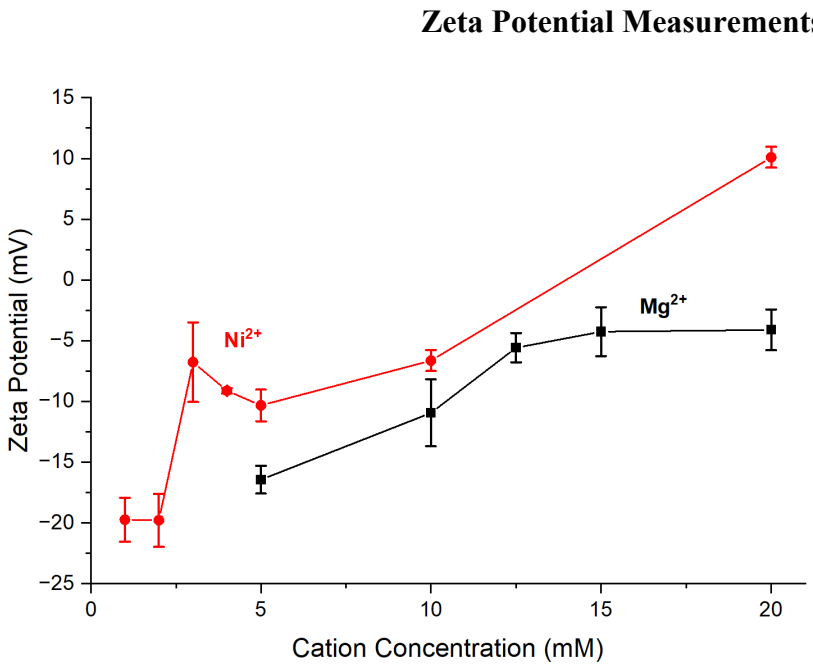

Figure S9. Effects of the divalent cation composition on the zeta potential (mV) of dsDNA. The concentration of Tris-Ac buffer was held constant at 4 mM.

To obtain zeta potential values from the target strand, we employed a previously reported diffusion barrier method with optimized measurement settings[13] to experimentally investigate the dependence of electrophoretic mobility/zeta potential on ionic strength, and the transition from low to high ionic strength in common buffer solutions. This method was chosen due to its ability to minimize sample volumes and isolate the dispersed phase from the electrode surface by filling the cell with a diffusion barrier. Disposable folded capillary cells (DTS1070) were typically filled with a mixture of 0.8 mL of the buffer being tested and a gel loading tip was then used to place a 20 µL aliquot of the dispersed phase, containing 5 ng/µL of the target strand dispersed in the same buffer solution under test. This mixture was then added exclusively to the optical detection volume at the bottom of the cell, away from the electrode surfaces. All batch data were recorded using a Zetasizer Pro instrument (Malvern Panalytical Ltd). Zeta potential values were measured using a monomodal analysis model with an equilibration time of 180 s, with a minimum of 10 runs and a maximum of 100 runs. All voltages and optical attenuation were set to automatic unless otherwise stated. Sub-runs were conducted at 25 °C with a 180 s pause between each measurement to allow for the dissipation of joule heating in the sample. For all measurements, each cell was thoroughly rinsed with methanol followed by generous amounts of deionized water. To prevent cross-contamination, a unique cell was used for each aliquot.

Computational Details

Charge transfer calculation:

The amount of charge transferred within each metal-ligand complex was calculated as the absolute change in the sum of partial atomic charges for the metal ion and explicit water molecules. Partial atomic charges were computed using the iterative Hirshfeld scheme;[14-15] this partial atomic charge method has been shown to accurately model both the dipole moment of water clusters and the charge transfer between water molecules.[16]

Validation of computational methods:

The optimized structures of $Mg^{2+}(H_2O)_6$, $Ni^{2+}(H_2O)_6$, and $Co^{2+}(H_2O)_6$ reproduce experimental ion-water oxygen distances ($d_{ion\text{-}O}$) within 0.10 Å (Table S1). The experimental binding free energy of Mg^{2+} bound to surface-bound single-strand DNA (approximately 8 kcal/mol)[17] is also reproduced (Table S2). Although numerical agreement is improved by omitting empirical dispersion, the trends in the relative binding energies are consistent with and without empirical dispersion (Table S2).

Table S1. Experimental and calculated ion-water oxygen distance ($d_{ion\text{-}O}$) values (Å) for $Mg^{2+}(H_2O)_6$, $Ni^{2+}(H_2O)_6$, and $Co^{2+}(H_2O)_6$.

metal ion	experiment	calculated[a]
Mg^{2+}	2.066[b]	2.11 ± 0.01
Ni^{2+}	2.05-2.065[c]	2.09 ± 0.01
Co^{2+}	2.08-2.09[c]	2.18 ± 0.01

a Average $d_{ion\text{-}O}$ value with the largest absolute difference between calculated $d_{ion\text{-}O}$ values and the average $d_{ion\text{-}O}$ value.
b Reference 18.
c References 18-20.

Table S2. Calculated binding energies (kcal/mol) of $Mg^{2+}(H_2O)_6$ indirectly and directly bound to carboxylate, phosphate, or guanine with and without empirical dispersion.[a]

ligand	binding motif	with dispersion	without dispersion
carboxylate	indirect	–19.0	–14.4
	direct	–10.4	–7.9
phosphate	indirect	–19.6	–12.3

	direct	–11.5	–6.5
guanine	indirect	–14.9	–9.2
	direct (N7)	–7.6	–2.5
	direct (O6)	–6.9	–2.8
average (phosphate and guanine)[b]		–12.8 ± 4.7	–6.7 ± 3.8

a Single-point energies calculated at the B3LYP/6-311+g(d,p) level of theory with and without GD3BJ empirical dispersion for molecular geometries optimized at the same level of theory with GD3BJ empirical dispersion.
b Mean and standard deviation of calculated binding energies for all phosphate and guanine binding sites and motifs.

Binary metal-ligand complexes:

The binding energies of Mg^{2+}, Ni^{2+}, and Co^{2+} bound to carboxylate, phosphate, or guanine and the optimized structures of these binary Mg^{2+} complexes are shown in Figure 6. The molecular structures of these complexes are similar for all ions studied. Indirect binding occurs through three hydrogen bonds between water molecules within the first solvation shell of the metal ion and carboxylate, phosphate, or guanine. Direct binding is monodentate and accompanied by two hydrogen bonds for carboxylate and phosphate. Guanine has two binding sites, namely, the N7 and the O6 atoms. Indirectly bound ions form two hydrogen bonds to O6 and one hydrogen bond to N7 simultaneously. Direct binding to guanine is also monodentate and may occur at either the O6 atom with one hydrogen bond to N7 or the N7 atom with two hydrogen bonds to O6. Bidentate binding structures are also stable for guanine with one direct contact to O6 and N7 and no hydrogen bonds, but one water molecule moves to the second solvation shell of the metal ion and this binding motif is not considered further.

Ternary metal-ligand complexes:

The binding energies of Mg^{2+}, Ni^{2+}, and Co^{2+} simultaneously bound to either carboxylate and phosphate or carboxylate and guanine and the optimized structures of the ternary Mg^{2+} complexes are shown in Figure S7. The structures of the Ni^{2+} and Co^{2+} ternary complexes are similar to those of Mg^{2+}. The ternary metal-ligand complexes yield similar binding motifs and relative binding energies as the binary complexes and are not considered further.

Absolute energies of optimized structures:

Structure	Binding	Species	Absolute energy (hartree)
Monomer	n/a	H_2O	-76.4725953444
		CH_3COO^-	-228.722813507
		$(CH_3)_2PO_4^-$	-722.492282676
		2-amino-9*H*-purin-6(1*H*)-one	-542.785419230
		$[Mg(H_2O)_6]^{2+}$	-658.853061207
		$[Ni(H_2O)_6]^{2+}$	-1966.95704264
		$[Co(H_2O)_6]^{2+}$	-1841.43332049
Dimer	Indirect	$[Mg(H_2O)_6\,CH_3COO]^+$	-887.608140293
		$[Ni(H_2O)_6\,CH_3COO]^+$	-2195.71354929
		$[Co(H_2O)_6\,CH_3COO]^+$	-2070.18759745
		$[Mg(H_2O)_6\,(CH_3)_2PO_4]^+$	-1381.38056318
		$[Ni(H_2O)_6\,(CH_3)_2PO_4]^+$	-2689.48568071
		$[Co(H_2O)_6\,(CH_3)_2PO_4]^+$	-2563.95952517
		$[Mg(H_2O)_6$ 2-amino-9*H*-purin-6(1*H*)-one$]^{2+}$	-1201.66446601
		$[Ni(H_2O)_6$ 2-amino-9*H*-purin-6(1*H*)-one$]^{2+}$	-2509.77071651
		$[Co(H_2O)_6$ 2-amino-9*H*-purin-6(1*H*)-one$]^{2+}$	-2384.24383819
Dimer	Direct	$[Mg(H_2O)_5\,CH_3COO]^+$	-811.122726708
		$[Ni(H_2O)_5\,CH_3COO]^+$	-2119.2290979
		$[Co(H_2O)_5\,CH_3COO]^+$	-1993.70382444
		$[Mg(H_2O)_5\,(CH_3)_2PO_4]^+$	-1304.89612356
		$[Ni(H_2O)_5\,(CH_3)_2PO_4]^+$	-2613.00015179
		$[Co(H_2O)_5\,(CH_3)_2PO_4]^+$	-2487.47396847
		$[Mg(H_2O)_5$ 2-amino-9*H*-purin-6(1*H*)-one$]^{2+}$	-1125.18139879[a] -1125.17973816[b]
		$[Ni(H_2O)_5$ 2-amino-9*H*-purin-6(1*H*)-one$]^{2+}$	-2433.29400425[a] -2433.28413954[b]
		$[Co(H_2O)_5$ 2-amino-9*H*-purin-6(1*H*)-one$]^{2+}$	-2307.76363359[a] -2307.75650164[b]

a Metal cation is directly bound to the N7 atom of guanine.
b Metal cation is directly bound to the O6 atom of guanine.

Structure	Binding	Species	Absolute energy (hartree)
Trimer	Indirect	$[Mg(H_2O)_6\ CH_3COO\ (CH_3)_2PO_4]$	-1610.13485300
		$[Ni(H_2O)_6\ CH_3COO\ (CH_3)_2PO_4]$	-2918.24015981
		$[Co(H_2O)_6\ CH_3COO\ (CH_3)_2PO_4]$	-2792.71163632
		$[Mg(H_2O)_6\ CH_3COO$ 2-amino-9*H*-purin-6(1*H*)-one$]^+$	-1430.41910385
		$[Ni(H_2O)_6\ CH_3COO$ 2-amino-9*H*-purin-6(1*H*)-one$]^+$	-2738.52621141
		$[Co(H_2O)_6\ CH_3COO$ 2-amino-9*H*-purin-6(1*H*)-one$]^+$	-2612.99795142
Trimer	Direct	$[Mg(H_2O)_4\ CH_3COO\ (CH_3)_2PO_4]$	-1457.16404555
		$[Ni(H_2O)_4\ CH_3COO\ (CH_3)_2PO_4]$	-2765.27083689
		$[Co(H_2O)_4\ CH_3COO\ (CH_3)_2PO_4]$	-2639.74461654
		$[Mg(H_2O)_4\ CH_3COO$ 2-amino-9*H*-purin-6(1*H*)-one$]^+$	-1277.45134538[a]
		$[Ni(H_2O)_4\ CH_3COO$ 2-amino-9*H*-purin-6(1*H*)-one$]^+$	-2585.56489939[a]
		$[Co(H_2O)_4\ CH_3COO$ 2-amino-9*H*-purin-6(1*H*)-one$]^+$	-2460.03421097[a]

a Metal cation is directly bound to the N7 atom of guanine.

REFERENCES

1. Abel, G. R., Jr.; Josephs, E. A.; Luong, N.; Ye, T., A switchable surface enables visualization of single DNA hybridization events with atomic force microscopy. *J Am Chem Soc* **2013,** *135* (17), 6399-402.
2. Abel, G. R., Jr.; Cao, B. H.; Hein, J. E.; Ye, T., Covalent, sequence-specific attachment of long DNA molecules to a surface using DNA-templated click chemistry. *Chem Commun (Camb)* **2014,** *50* (60), 8131-3.
3. Gamboa Varela, J.; Gates, K. S., A simple, high-yield synthesis of DNA duplexes containing a covalent, thermally cleavable interstrand cross-link at a defined location. *Angew Chem Int Ed Engl* **2015,** *54* (26), 7666-9.
4. Fuentes, R.; Morgan, L.; Matwiyoff, N., Fourier transform carbon-13 nuclear magnetic resonance of aqueous nickel (II)-acetic acid solutions. I. Equilibrium quotients from relative abundances of solution species. *Inorg Chem* **1975,** *14* (8), 1837-1840.
5. Heinz, H.; Jha, K. C.; Luettmer-Strathmann, J.; Farmer, B. L.; Naik, R. R., Polarization at metal-biomolecular interfaces in solution. *J R Soc Interface* **2011,** *8* (55), 220-232.
6. Geada, I. L.; Ramezani-Dakhel, H.; Jamil, T.; Sulpizi, M.; Heinz, H., Insight into induced charges at metal surfaces and biointerfaces using a polarizable Lennard-Jones potential. *Nat Commun* **2018,** *9*, 716.
7. Manning, G. S., The molecular theory of polyelectrolyte solutions with applications to the electrostatic properties of polynucleotides. *Quarterly reviews of biophysics* **1978,** *11* (2), 179-246.
8. Son, C. Y.; Wang, Z. G., Image-charge effects on ion adsorption near aqueous interfaces. *P Natl Acad Sci USA* **2021,** *118* (19), 2020615118.
9. Simon-Kutscher, J.; Gericke, A.; Huhnerfuss, H., Effect of bivalent Ba, Cu, Ni, and Zn cations on the structure of octadecanoic acid monolayers at the air-water interface as determined by external infrared reflection-absorption spectroscopy. *Langmuir* **1996,** *12* (4), 1027-1034.
10. Wang, Y. C.; Du, X. Z.; Guo, L.; Liu, H. J., Chain orientation and headgroup structure in Langmuir monolayers of stearic acid and metal stearate (Ag, Co, Zn, and Pb) studied by infrared reflection-absorption spectroscopy. *J Chem Phys* **2006,** *124* (13), 134706.
11. Bala, T.; Prasad, B. L. V.; Sastry, M.; Kahaly, M. U.; Waghmare, U. V., Interaction of different metal ions with carboxylic acid group: A quantitative study. *J Phys Chem A* **2007,** *111* (28), 6183-6190.
12. Rouzina, I.; Bloomfield, V. A., Macroion attraction due to electrostatic correlation between screening counterions .1. Mobile surface-adsorbed ions and diffuse ion cloud. *J Phys Chem* **1996,** *100* (23), 9977-9989.
13. Austin, J.; Fernandes, D.; Ruszala, M. J. A.; Hill, N.; Corbett, J., Routine, ensemble characterisation of electrophoretic mobility in high and saturated ionic dispersions. *Sci Rep* **2020,** *10* (1).
14. Hirshfeld, F. L., Bonded-Atom Fragments for Describing Molecular Charge-Densities. *Theor Chim Acta* **1977,** *44* (2), 129-138.
15. Bultinck, P.; Van Alsenoy, C.; Ayers, P. W.; Carbo-Dorca, R., Critical analysis and extension of the Hirshfeld atoms in molecules. *J Chem Phys* **2007,** *126* (14), 144111.
16. Han, B. W.; Isborn, C. M.; Shi, L., Determining Partial Atomic Charges for Liquid Water: Assessing Electronic Structure and Charge Models. *J Chem Theory Comput* **2021,** *17* (2), 889-901.

17. Holland, J. G.; Jordan, D. S.; Geiger, F. M., Divalent Metal Cation Speciation and Binding to Surface-Bound Oligonucleotide Single Strands Studied by Second Harmonic Generation. *J Phys Chem B* **2011,** *115* (25), 8338-8345.
18. Ohtaki, H.; Radnai, T., Structure and Dynamics of Hydrated Ions. *Chem Rev* **1993,** *93* (3), 1157-1204.
19. Inada, Y.; Hayashi, H.; Sugimoto, K.; Funahashi, S., Solvation structures of Manganese(II), iron(II), cobalt(II), nickel(II), copper(II), zinc(II), and gallium(III) ions in methanol, ethanol, dimethyl sulfoxide, and trimethyl phosphate as studied by EXAFS and electronic spectroscopies. *J Phys Chem A* **1999,** *103* (10), 1401-1406.
20. D'Angelo, P.; Barone, V.; Chillemi, G.; Sanna, N.; Meyer-Klaucke, W.; Pavel, N. V., Hydrogen and higher shell contributions in Zn2+, Ni2+, and Co2+ aqueous solutions: An X-ray absorption fine structure and molecular dynamics study. *J Am Chem Soc* **2002,** *124* (9), 1958-1967.